Vibrational Spectroscopy of Intermediates in Benzene-to-Pheno Conversion by FeO^+

Gokhan Altinay and Ricardo B. Metz
Department of Chemistry, University of Massachusetts Amherst, Amherst, Massachusetts, USA

Gas-phase FeO^+ can convert benzene to phenol under thermal conditions. Two key intermediates of this reaction are the $[HO\text{-}Fe\text{-}C_6H_5]^+$ insertion intermediate and $Fe^+(C_6H_5OH)$ exit channel complex. These intermediates are selectively formed by reaction of laser ablated Fe^+ with specific organic precursors and are cooled in a supersonic expansion. Vibrational spectra of the sextet and quartet states of the intermediates in the O–H stretching region are measured by infrared multiphoton dissociation (IRMPD). For $Fe^+(C_6H_5OH)$, the O–H stretch is observed at 3598 cm^{-1}. Photodissociation primarily produces $Fe^+ + C_6H_5OH$; $Fe^+(C_6H_4) + H_2O$ is also observed. IRMPD of $[HO\text{-}Fe\text{-}C_6H_5]^+$ mainly produces $FeOH^+ + C_6H_5$ and the O–H stretch spectrum consists of a peak at ~3700 cm^{-1} with a shoulder at ~3670 cm^{-1}. Analysis of the experimental results is aided by comparison with hybrid density functional theory computed frequencies. Also, an improved potential energy surface for the $FeO^+ + C_6H_6$ reaction is developed based on CBS-QB3 calculations for the reactants, intermediates, transition states, and products. (J Am Soc Mass Spectrom 2010, 21, 750–757) © 2010 Published by Elsevier Inc. on behalf of American Society for Mass Spectrometry

Phenol is an important commodity chemical, with 9 million metric tons produced worldwide. It is used to make materials such as polycarbonate, nylon, and epoxy resins, drugs such as aspirin, and cosmetics such as sunscreens and hair dyes [1]. Industrially, phenol is mainly produced from benzene via the cumene process: benzene → cumene → cumene hydroperoxide → phenol. This three-step process is energy intensive and has a low phenol yield. Thus, direct conversion of benzene to phenol has attracted great attention due to its economical and industrial importance. Promising direct benzene-phenol oxidation techniques include Fe-doped ZSM-5 zeolites with N_2O as the oxidant [2, 3] and direct oxidation using O_2 and H_2 through a Pd membrane [4]. Some bacteria can directly convert benzene to phenol under mild conditions using toluene monooxygenases, which have a di-iron active site [5]. The biotoxicity of benzene in mammals is enhanced by its conversion to phenol by cytochrome P450, which has an Fe-heme active site [6, 7].

Schwarz and coworkers showed that under thermal conditions, several gas-phase metal oxide cations MO^+ react efficiently with benzene to produce phenol with good selectivity [8]. The reaction of FeO^+ has been particularly well-studied. It primarily produces Fe^+ + phenol (56%) and $Fe(C_5H_6)^+ + CO$ (37%) [9]. They subsequently produced several $[FeC_6H_6O]^+$ isomers by reacting Fe^+ with different precursors in a chemical ionization source and characterized them using fragmentation patterns observed following collisional activation in a tandem mass spectrometer [10].

This prototypical arene oxidation reaction has also been studied computationally. Yoshizawa et al. calculated the energetics of reactants, intermediates and transition states for benzene-phenol conversion by FeO^+ using B3LYP hybrid density functional theory [11]. They considered a mechanism in which FeO^+ first binds to the ring, forming a $OFe^+(C_6H_6)$ entrance channel complex, then hydrogen abstraction via transition-state TS1 forms the insertion intermediate $HO\text{-}Fe^+\text{-}C_6H_5$. Phenyl or hydroxyl migration through TS2 produces the $Fe^+(C_6H_5OH)$ exit channel complex, which subsequently dissociates to $Fe^+ + C_6H_5OH$. Molecular dynamics simulations on this potential energy surface predict that the reaction is rapid, and that the hydrogen transfer at TS1 leads to O–H stretch excitation in the insertion intermediate [12]. They later also considered two other possible mechanisms. A radical mechanism involving direct H atom abstraction via a Fe-O–H transition-state was considered unlikely on energetic grounds. An oxygen insertion mechanism that proceeds via an arenium intermediate $[FeOC_6H_6]^+$ with covalent Fe–O–C bonds was considered to be favorable if the FeO^+ was also ligated [13]. The oxygen insertion mechanism was also studied by Kwapien and Broclawik [14].

Our group has studied the vibrational and electronic spectroscopy of intermediates of methane to methanol conversion by FeO^+ [15, 16]. By extending these studies to benzene-phenol conversion by FeO^+, we can evalu-

Address reprint requests to Professor R. B. Metz, Department of Chemistry, University of Massachusetts Amherst, Amherst, MA 01003, USA. E-mail: rbmetz@chem.umass.edu

1044-0305/10/$32.00
doi:10.1016/j.jasms.2010.01.006

Published online January 25, 2010
Received December 1, 2009
Revised January 7, 2010
Accepted January 7, 2010

ate the effect of the aromatic ring on the reaction mechanism.

Experimental and Theoretical Methods

Vibrational spectra are measured using a dual time-of-flight reflectron photofragment spectrometer [17, 18]. Iron cations are generated by laser ablation of an iron rod (Sigma-Aldrich, St. Louis, MO, USA, 99.8% pure). Fe^+ cations react with either 0.01% phenol in helium or a mixture of 2% N_2O and 0.5% benzene in helium to produce the target molecule. The choice of precursors is guided by the collisional activation (CA) studies of Becker et al. [10], and is discussed in more detail below. Ions produced in the source expand supersonically into vacuum and cool to a rotational temperature of ~10 K [19]. Ions are accelerated to 1800 V kinetic energy, then re-referenced to ground potential before entering the field-free flight tube. Mass-selected ions are photodissociated at the turning point of the reflectron. Energetically, photodissociation of $[HO\text{-}Fe\text{-}C_6H_5]^+$ requires at least four photons in the O–H stretching region. So, vibrational spectra are obtained using infrared multiphoton dissociation (IRMPD) of $[HO\text{-}Fe\text{-}C_6H_5]^+$ and $Fe^+(C_6H_5OH)$. The photodissociation efficiency is greatly improved using a multi-pass mirror arrangement [20] in which the laser makes 21 passes through the ion cloud. The light source is a Nd:YAG pumped optical parametric oscillator, which is tunable from 2 to 5 μm, producing ~10 mJ/pulse near 3600 cm^{-1}. The IR beam path is purged with nitrogen to minimize absorptions by water vapor. The laser wavelength is calibrated using H_2O absorptions. Fragment ions and undissociated parent ions are detected by a dual micro-channel plate detector. The ion signal is amplified, collected on a digital oscilloscope, or a gated integrator, and averaged with a LabView based program. The photodissociation spectrum is obtained by monitoring the yield of the fragment ion of interest as a function of wavelength and normalizing to parent ion signal and laser fluence. In this study, we separately and simultaneously monitor the Fe^+ and $FeOH^+$ fragments. The photodissociation spectrum is the product of the absorption spectrum and the photodissociation quantum yield.

Computations are carried out with the Gaussian 2003 program package [21]. Optimized geometries of the reactants, intermediates, transition states, and products are calculated using the Becke-Lee-Yang-Parr hybrid HF/DFT method (B3LYP) with the 6-311+G(d,p) basis set. Vibrational frequencies are computed to ensure that all optimized geometries correspond to a local minimum or a first-order saddle point (for transition states). To obtain more accurate energies, we calculated single-point energies using the complete basis set CBS-QB3 method, which is optimized for thermodynamics [22, 23]. All energies include zero point energy and correspond to 0 Kelvin values.

Results and Discussion

Potential Energy Surface for the $FeO^+ + C_6H_6$ Reaction

To establish the accuracy of the computational method used, we compare calculated and accurate experimental results for the sextet-quartet energy splitting in Fe^+, the Fe^+–O bond enthalpy, and the overall exothermicity of the $FeO^+ + C_6H_6 \rightarrow Fe^+ + C_6H_5OH$ reaction. Experimentally, the ground state of Fe^+ is ^6D ($3d^6\,4s$), with the ^4F ($3d^7$) state 23.9 kJ/mol higher. Calculations at the B3LYP/6-311+G(d,p) level incorrectly predict a quartet ground state, 19.8 kJ/mol below the sextet state. This is a well known failure of the B3LYP method [24, 25]. An attractive alternative to rigorous and expensive high level correlated ab initio calculations are hybrid methods developed for accurate thermochemistry, such as the complete basis set CBS-QB3 approach [22, 23]. In CBS-QB3, one first optimizes the geometry and calculates harmonic frequencies at the B3LYP level. Then, from a series of single point energy calculations at various levels of theory and with different basis sets, one extrapolates the result of a large basis set calculation at a very high level of theory. CBS-QB3 thermodynamics have similar accuracy to an extrapolated series of CCSD(T) calculations with very large basis sets, and are significantly more accurate than a single CCSD(T) calculation with a modest basis set [26]. CBS-QB3 calculations correctly predict the ordering of the Fe^+ states, with the quartet 30.1 kJ/mol above the sextet. For the dissociation enthalpy of FeO^+, CBS-QB3 calculations predict 337.8 kJ/mol, in excellent agreement with experiment (340 ± 2 kJ/mol [27]; 335 ± 5 kJ/mol [28]). For the $FeO^+ + C_6H_6 \rightarrow Fe^+ + C_6H_5OH$ reaction enthalpy, CBS-QB3 predicts −88 kJ/mol, in excellent agreement with experiment, −85 ± 2 kJ/mol [27, 29].

Figure 1 shows the potential energy surface for the $FeO^+ + C_6H_6$ reaction calculated using the CBS-QB3 method. Phenol production occurs in a two-step concerted manner through the formation of the hydroxy intermediate $[HO\text{-}Fe\text{-}C_6H_5]^+$. The minimum energy path involves first producing the $OFe^+(C_6H_6)$ entrance channel complex. For the sextet state, the FeO^+ is not centered on the ring, but rather binds to adjacent carbons in a η_2 configuration, with r(Fe-C) = 2.34 Å. Quartet FeO^+ is nearly centered on the ring, with r(Fe-C) = 2.32 Å. Hydrogen abstraction via TS1 leads to the key $[HO\text{-}Fe\text{-}C_6H_5]^+$ insertion intermediate. For the quartet state, the Fe-O–H group is perpendicular to the ring, with r(Fe-C) = 1.878 Å, r(Fe-O) = 1.705 Å, and r(O–H) = 0.964 Å. In the sextet state, the Fe-O–H group is in the plane of the ring, with slightly longer bonds to iron: with r(Fe-C) = 1.908 Å, r(Fe-O) = 1.729 Å and r(O–H) = 0.961 Å. The FeO^+ reactant and Fe^+ product have sextet ground states [19]. The minimum energy pathway involves quartet intermediates. However, since both sextet TS1 and sextet TS2 lie below the reactants, the reaction can proceed completely along the

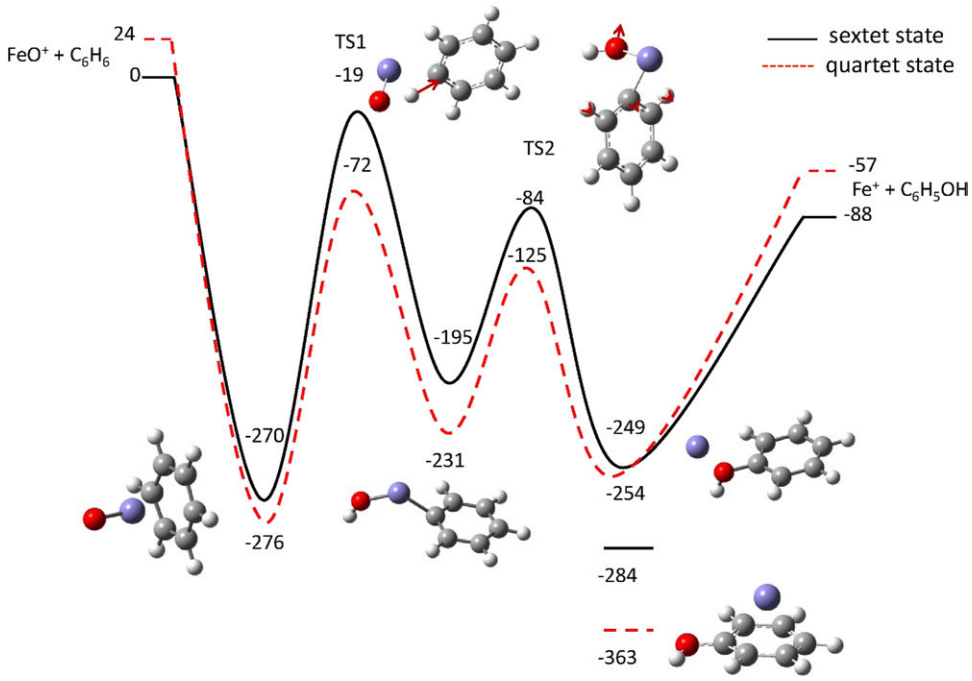

Figure 1. Schematic potential energy surface for the $FeO^+ + C_6H_6 \rightarrow Fe^+ + C_6H_5OH$ reaction and structures of intermediates and transition states. Energies (in kJ/mol) are calculated at the CBS-QB3 level of theory. The solid line represents the sextet and dashed line the quartet surface. The imaginary frequencies for transition states TS1 and TS2 are 1930*i* and 390*i* for quartet states and 1916*i* and 352*i* for sextet states, respectively. The corresponding vibrations are shown with red arrows in the figure. All geometries shown are those of the quartet states.

sextet pathway without changing spin. The overall reaction efficiency is determined by the probability that reactants will cross TS1, which can occur in two ways: by crossing sextet TS1, or by changing spin and crossing the low-lying quartet TS1. This is a major difference from the FeO^+ + methane reaction, where sextet TS1 lies above reactants. As a result, FeO^+ reacts with benzene at the collision rate [9], while it reacts with methane at only ~20% of the collision rate [30, 31]. Once produced, the $[HO\text{-}Fe\text{-}C_6H_5]^+$ insertion intermediate can isomerize via TS2 to form the $Fe^+(C_6H_5OH)$ exit channel complex, which subsequently dissociates to $Fe^+ + C_6H_5OH$. The calculations predict that production of $FeOH^+ + C_6H_5$ is 20 kJ/mol endothermic. So, it is not surprising that is not observed as a product of the $FeO^+ + C_6H_6$ reaction [9]. This is another significant difference with the $FeO^+ + CH_4$ system, where $FeOH^+ + CH_3$ is energetically allowed, is a significant product at thermal energies, and dominates at high collision energy [31]. Manganese is the only first-row transition-metal for which MOH^+ is observed as a product of the MO^+ + benzene reaction [8]. The calculations predict two isomers of the $Fe^+(C_6H_5OH)$ exit channel complex. A σ-complex in which the Fe^+ binds to the oxygen lone pair, and a π-complex, where the Fe^+ binds to the ring. The π-complex is predicted to lie lower in energy, at −284 kJ/mol (sextet state) and −363 kJ/mol (quartet state), relative to $FeO^+ + C_6H_6$. In the σ-complex, the Fe^+ is not in the plane of the ring, and is 1.952 Å from the oxygen for the quartet state. The Fe-O distance is substantially longer for the sextet state, at 2.071 Å. The quartet π-complex has a very interesting geometry. The carbons *ortho* and *meta* to the −OH group pucker towards the Fe^+, leading to η_4 coordination, with r(Fe-C) = 2.20 Å. Sextet Fe^+ binds much more weakly and leads to much less distortion of the ring. The Fe^+ is slightly displaced towards a *meta* carbon, with r(Fe-C) = 2.53 Å. The electron in the large 4s orbital leads to much weaker noncovalent interactions for sextet Fe^+ ($3d^6$ 4s electron configuration) than for quartet Fe^+ ($3d^7$ configuration). Our potential energy surface for the $FeO^+ + C_6H_6$ reaction is similar to one calculated by Yoshizawa et al. at the B3LYP/6-311+G(d,p) level [11]. One key difference is that the B3LYP calculations predict that the $[HO\text{-}Fe\text{-}C_6H_5]^+$ insertion intermediates are ~20 kJ/mol more stable relative to reactants. As a result, TS1 and TS2 are also predicted to be ~20 kJ/mol lower. Previous studies of the $FeO^+ + C_6H_6$ reaction have also considered two other mechanisms: a radical and an oxygen insertion mechanism [13, 14]. We measure the spectra of $[FeC_6H_6O]^+$ intermediates in the O–H stretching region. The C-H stretches are weak and they are not distinctive for different intermediates. We did not carry out calculations on the intermediates in the alternate mechanisms as they do not contain an O–H bond. In addition, as our experiments measure spectra in the O–H stretching region, we are not sensitive to the pres-

ence of other likely intermediates such as the $OFe^+(C_6H_6)$ entrance channel complex or the key arenium intermediate $[FeOC_6H_6]^+$ in the proposed oxygen insertion mechanism, as these species do not contain O–H bonds.

IRMPD Spectroscopy of $[FeC_6H_6O]^+$

A major challenge in studies of intermediates of ion-molecule reactions is to find suitable precursors and reaction conditions to selectively produce specific intermediates. The identity of the intermediates produced is deduced from their vibrational spectrum and dissociation pathways. Vibrational spectra of $[HO\text{-}Fe\text{-}C_6H_5]^+$ and $Fe^+(C_6H_5OH)$ in the O–H stretching region were measured using photofragment spectroscopy. A challenge in obtaining vibrational spectra using photofragment spectroscopy is that absorption of a photon needs to lead to bond breaking. One photon in the O–H stretching region only has ~43 kJ/mol of energy, so photodissociation of $[HO\text{-}Fe\text{-}C_6H_5]^+$ or $Fe^+(C_6H_5OH)$ requires at least four photons. So, vibrational spectra were measured using infrared multi-photon dissociation (IRMPD). We previously used IRMPD to measure vibrational spectra of the $[HO\text{-}Fe\text{-}CH_3]^+$ and $Fe^+(CH_3OH)$ intermediates of the $FeO^+ + CH_4 \rightarrow Fe^+ + CH_3OH$ reaction [15]. They are not ideal candidates for IRMPD due to the high binding energy and small size of the molecules, which leads to relatively slow intramolecular vibrational distribution (IVR) of energy. Intermediates of the $FeO^+ + C_6H_6$ reaction are much better suited to IRMPD studies, and we observe higher dissociation yields and significantly narrower spectra for the larger system.

In this study, we find that reacting ablated Fe^+ with phenol or benzene + N_2O produces $[HO\text{-}Fe\text{-}C_6H_5]^+$ and $Fe^+(C_6H_5OH)$, with the relative amounts depending on the precursor. IRMPD of ions generated by reacting Fe^+ with 0.01% phenol in helium primarily produces Fe^+ and $FeOH^+$ photofragments. Along with a small amount of $Fe^+(C_6H_4) + H_2O$, trace amounts of $Fe^+(C_5H_6)$ + CO and $Fe^+(C_5H_5)$ + HCO are also observed. The maximum dissociation yield is ~15%. Figure 2 (top) shows IRMPD spectra obtained by monitoring Fe^+ (blue) and $FeOH^+$ (red). The two channels give completely different vibrational spectra, indicating that two or more intermediates are produced in the source, and each channel monitors a different interme-

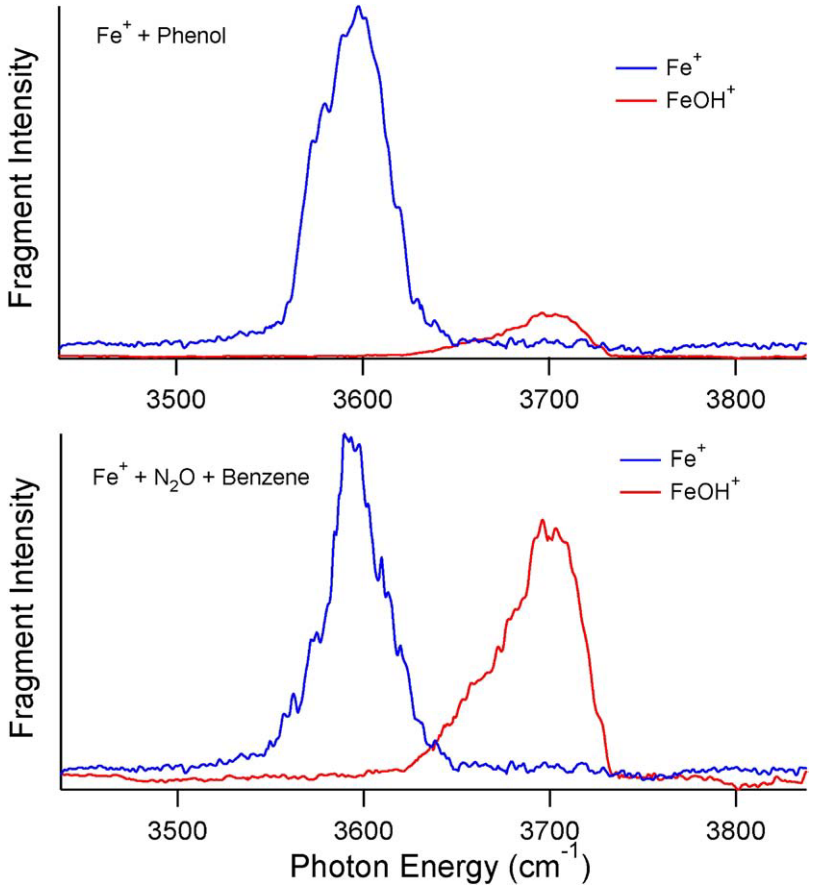

Figure 2. Vibrational spectra of $[FeC_6H_6O]^+$ in the O–H stretching region. Spectra are obtained by IRMPD of ions produced by reacting Fe^+ with C_6H_5OH (top) and by reacting Fe^+ with N_2O and C_6H_6 (bottom). Spectra obtained by monitoring Fe^+ and $FeOH^+$ are in blue and red, respectively. The two product channels are formed by dissociation of different $[FeC_6H_6O]^+$ isomers, and the relative amounts of these isomers depends on the precursor.

diate or group of intermediates. The $Fe^+(C_6H_4)$ and Fe^+ channels have a similar wavelength dependence. Photodissociation of $[FeC_6H_6O]^+$ ions produced using 0.5% benzene and 2% N_2O in helium also gives Fe^+ and $FeOH^+$ as the major fragments. Again, spectra obtained by monitoring Fe^+ and $FeOH^+$ are different (Figure 2, bottom). The observed dissociation products and vibrational frequencies (see below) indicate that IRMPD of $Fe^+(C_6H_5OH)$ produces $Fe^+ + C_6H_5OH$ while IRMPD of $[HO\text{-}Fe\text{-}C_6H_5]^+$ forms $FeOH^+ + C_6H_5$. Becker et al. generated several $[FeC_6H_6O]^+$ isomers by reacting Fe^+ produced by electron bombardment of $Fe(CO)_5$ with organic molecules in a chemical ionization source and characterized them by collisional activation (CA) [10]. CA of $Fe^+(C_6H_5OH)$ primarily leads to $Fe^+(C_6H_4) + H_2O$ and Fe^+ + phenol, while $Fe^+(C_5H_6)$ + CO and $FeOH^+ + C_6H_5$ are major products in CA of $[HO\text{-}Fe\text{-}C_6H_5]^+$. So, the fragment ions observed by CA and IRMPD are similar.

In the O–H stretching region, IRMPD of $[FeC_6H_6O]^+$ produced by reacting Fe^+ with phenol in helium produces $FeOH^+ + C_6H_5$ or $Fe^+ + C_6H_5OH$, depending on wavelength. The spectrum of $Fe^+(C_6H_5OH)$, obtained by monitoring Fe^+, consists of a 45 cm^{-1} FWHM peak at 3598 cm^{-1}. This is 59 cm^{-1} red shifted from the O–H stretch in bare phenol (3657 cm^{-1}) [32]. Under the same conditions, the $FeOH^+$ channel gives a much less intense, 50 cm^{-1} FWHM peak at ~3700 cm^{-1}. Dissociating $[FeC_6H_6O]^+$ formed by reacting Fe^+ with N_2O/benzene in helium also produces Fe^+ and $FeOH^+$. The relative intensity of the $FeOH^+$ channel increases 8-fold (Figure 2 bottom), but its peak position and shape are unchanged. This is consistent with reaction of Fe^+ with N_2O and benzene producing more $[HO\text{-}Fe\text{-}C_6H_5]^+$ than reaction of Fe^+ with phenol. The peak obtained by monitoring Fe^+ is slightly narrower for the N_2O/benzene precursor than for phenol. This suggests that more than one isomer or spin state of $Fe^+(C_6H_5OH)$ contributes to the spectrum or, more likely, that the ions have slightly different vibrational temperatures in the two cases. IRMPD spectra are more sensitive to internally excited molecules than one-photon spectroscopies, as fewer photons may be required to dissociate hot molecules.

To help assign the spectra, we calculated geometries, energies, and frequencies of the quartet and sextet states of insertion intermediate $[HO\text{-}Fe\text{-}C_6H_5]^+$ and exit channel complexes $Fe^+(C_6H_5OH)$ (Table 1). Calculations were carried out using the B3LYP hybrid density functional with the 6-311+G(d,p) basis set. Calculated harmonic frequencies are scaled by 0.954, which is the ratio of the experimental to calculated O–H stretching frequencies in bare phenol.

Vibrational Spectroscopy of the $[HO\text{-}Fe\text{-}C_6H_5]^+$ Insertion Intermediate

IRMPD of the $[HO\text{-}Fe\text{-}C_6H_5]^+$ insertion intermediate produces $FeOH^+ + C_6H_5$. Reacting laser-ablated Fe^+ with N_2O and benzene produces significantly more $[HO\text{-}Fe\text{-}C_6H_5]^+$ than does reaction with phenol. Both precursors lead to a vibrational spectrum with a peak at ~3700 cm^{-1} and a shoulder at ~3670 cm^{-1} (red traces in Figure 2 and Figure 3). The calculations predict O–H stretch vibrations at 3700 cm^{-1} and 3674 cm^{-1} for the sextet and quartet states of the insertion intermediate, respectively. The sextet has somewhat higher oscillator strength, while the quartet is predicted to lie 36 kJ/mol lower in energy. Both spin states appear to contribute to the spectrum: the peak at 3700 cm^{-1} is due to the sextet state, and the quartet state is responsible for the shoulder at ~3670 cm^{-1}. In our study of the insertion intermediate for the $FeO^+ + CH_4$ reaction, we also found that both spin states contribute to the vibrational spectrum. IRMPD of $[HO\text{-}Fe\text{-}CH_3]^+$ gives an asymmetrical peak at 3623 cm^{-1} with a shoulder at 3576 cm^{-1}, which were assigned to the sextet and quartet states, respectively [15]. Adding argon atoms to $[HO\text{-}Fe\text{-}CH_3]^+$ removes charge from the metal center and leads to progressively larger blue shifts in the O–H stretch frequencies. The O–H stretch in neutral $HO\text{-}Fe\text{-}CH_3$ shows an even larger blue shift, to 3745 cm^{-1} [33, 34]. Mulliken population analysis shows a charge of +0.77 for the Fe-O–H moiety in $[HO\text{-}Fe\text{-}CH_3]^+$, which drops to 0.56 in $[HO\text{-}Fe\text{-}C_6H_5]^+$. Relative to $[HO\text{-}Fe\text{-}CH_3]^+$, the O–H stretches of $[HO\text{-}Fe\text{-}C_6H_5]^+$ exhibit a ~80 cm^{-1} blue shift. Thus, this system continues a trend we

Table 1. Harmonic vibrational frequencies for intermediates of the $FeO^+ + C_6H_6 \rightarrow Fe^+ + C_6H_5OH$ reaction at the B3LYP/6-311+G(d,p) level. IR intensities (km/mol) in parentheses. Frequencies are scaled by 0.954

	O–H stretches (cm^{-1})	C–H stretches (cm^{-1})
C_6H_5OH	3657(61)	3049(4), 3042(17), 3029(17), 3003(14)
$OFe^+(C_6H_6)$ quartet	—	3063(0), 3058(42), 3050(0), 3049(0), 3044(0)
$OFe^+(C_6H_6)$ sextet	—	3064(5), 3057(13), 3053(9), 3048(3), 3045(3), 3037(0)
$[HO\text{-}Fe\text{-}C_6H_5]^+$ quartet	3674(467)	3056(2), 3050(3), 3041(1), 3027(5)
$[HO\text{-}Fe\text{-}C_6H_5]^+$ sextet	3700(849)	3058(1), 3052(0), 3041(0), 3027(0), 3016(0)
$Fe^+(C_6H_5OH)$ quartet π-structure	3619(158)	3063(3), 3059(10), 3052(1), 3047(0), 3032(1)
$Fe^+(C_6H_5OH)$ sextet π-structure	3617(175)	3065(7), 3058(14), 3051(3), 3046(1), 3033(2)
$Fe^+(C_6H_5OH)$ quartet σ-structure	3605(195)	3060(0), 3054(0), 3046(1), 3039(0), 3037(1)
$Fe^+(C_6H_5OH)$ sextet σ-structure	3562(173)	3061(0), 3056(0), 3048(0), 3042(1), 3039(7)

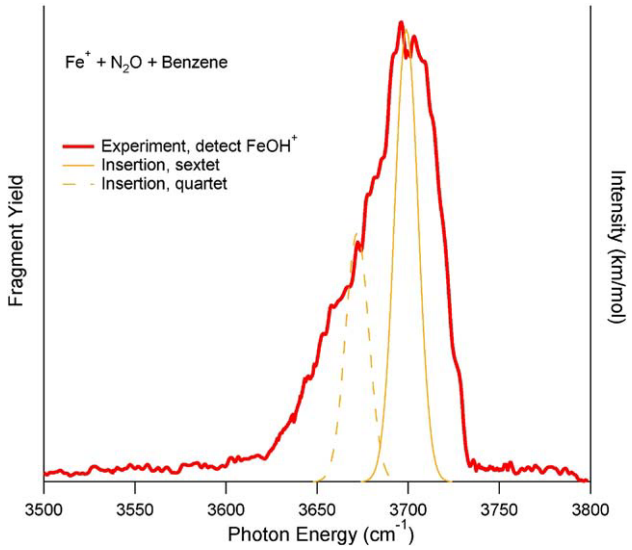

Figure 3. Experimental and calculated vibrational spectra of $[HO\text{-}Fe\text{-}C_6H_5]^+$ in the O–H stretching region. The experimental spectrum is obtained by IRMPD of ions produced by reacting Fe^+ with N_2O and C_6H_6 and monitoring $FeOH^+$ fragments (red). Calculated spectra (right axis) are at the B3LYP/6-311+G(d,p) level, with frequencies scaled by 0.954. For the simulations, solid lines represent sextet states and dashed lines quartet states.

observed previously: removing charge from the Fe-O–H group blue-shifts the O–H stretch frequency.

Our spectroscopic observation that reaction of Fe^+ with N_2O and benzene produces $[HO\text{-}Fe\text{-}C_6H_5]^+$ is a bit surprising in light of CA and ion cyclotron resonance (ICR) studies, which find no clear evidence for the $[HO\text{-}Fe\text{-}C_6H_5]^+$ intermediate in the $FeO^+ + C_6H_6$ reaction [8–10]. A possible explanation is that this reaction can occur via several mechanisms and the different conditions in our laser ablation source and in the ICR favor different reaction pathways. Our IRMPD results do not address whether other intermediates, such as the $OFe^+(C_6H_6)$ entrance channel complex or intermediates proposed for the oxygen insertion mechanism [13, 14], are also present. These intermediates do not contain an O–H bond and thus would not be detected in our study. Another possibility is that, in our laser ablation source, $[HO\text{-}Fe\text{-}C_6H_5]^+$ is not produced by

$$Fe^+ + N_2O \rightarrow FeO^+ + N_2 \quad (1)$$

followed by reaction of FeO^+ with benzene, but rather is formed by

$$Fe^+ + C_6H_6 \rightarrow Fe^+(C_6H_6) \quad (2)$$

followed by reaction of $Fe^+(C_6H_6)$ with N_2O. Although we use a 4:1 N_2O:C_6H_6 ratio, kinetics favors reaction 2. The high-pressure limiting bimolecular rate k_2 is 1.2×10^{-9} cm^3 $molecule^{-1}s^{-1}$ for Co^+ and should be similar for Fe^+ [8]. At thermal energies reaction 1 is much slower: [35] $k_1 = 3.1 \times 10^{-11}$ cm^3 $molecule^{-1}s^{-1}$. However, CID and ICR reaction studies [36] as well as flow tube studies [37] show that the $Fe^+(C_6H_6) + N_2O$ reaction produces $OFe^+(C_6H_6)$ (the entrance channel complex in Figure 1) rather than the insertion intermediate. Our spectroscopic results show that reacting laser-ablated Fe^+ with N_2O and benzene produces $[HO\text{-}Fe\text{-}C_6H_5]^+$. However, our experiments do not determine whether $[HO\text{-}Fe\text{-}C_6H_5]^+$ is formed by reaction of FeO^+ with benzene, or by reaction of Fe^+(benzene) with N_2O.

Vibrational Spectroscopy of the $Fe^+(C_6H_5OH)$ Exit Channel Complex

The $Fe^+(C_6H_5OH)$ exit channel complexes are predicted to have the lowest O–H stretching frequencies, with two different possible geometries. The Fe^+ can bind above the benzene ring (π-complex) or to the oxygen lone pair (σ-complex). The CBS-QB3 calculations predict that the lowest energy structure is clearly the quartet state of the π-complex, which is predicted to be bound by 275 kJ/mol relative to sextet Fe^+ + phenol. The sextet π-complex is bound by 196 kJ/mol, while the quartet and sextet σ-complexes are bound by 166 and 161 kJ/mol, respectively. The preference for Fe^+ to bind to the aromatic ring rather than to oxygen is consistent with the greater measured binding energy for Fe^+-benzene (207 ± 10 kJ/mol) than for Fe^+-H_2O (128 ± 5 kJ/mol) [38]. The quartet and sextet π-complexes and quartet σ-complex are predicted to have very similar O–H stretching frequencies. All are in excellent agreement with the observed O–H stretch at 3598 cm^{-1} (Figure 4). The O–H stretch for the sextet σ-complex is predicted to lie well below the observed peak.

The O–H stretching frequency in Fe^+(phenol) is 3598 cm^{-1}, which is 59 cm^{-1} below the O–H stretch in bare phenol (3657 cm^{-1}) [32]. Vaden and Lisy measured vibrational spectra of M^+(phenol)(Ar) (M = Na, K) in the O–H stretching region, monitoring argon loss [39]. For K^+ they observed a narrow, symmetric peak at 3636 cm^{-1}, which was assigned to the π-complex. The spectrum of the Na^+ complex consists of a peak at 3641 cm^{-1} with a clear shoulder at 3632 cm^{-1}, which were assigned to the σ- and π-complexes, respectively. So, binding to Na^+ or K^+ leads to a ~20 cm^{-1} red shift in the O–H stretching frequency of bare phenol; significantly smaller than the 59 cm^{-1} red shift due to Fe^+ binding. The observed red shifts correlate with the binding energies of M^+(phenol), which are measured [40] to be 74 kJ/mol for K^+, 102 kJ/mol for Na^+, and calculated to be 275 kJ/mol for Fe^+. Recent IRMPD experiments in the fingerprint region show that Ag^+ also forms a π-complex with phenol [41].

Conclusions

Vibrational spectra of two intermediates of the gas-phase $FeO^+ + C_6H_6 \rightarrow Fe^+ + C_6H_5OH$ reaction have

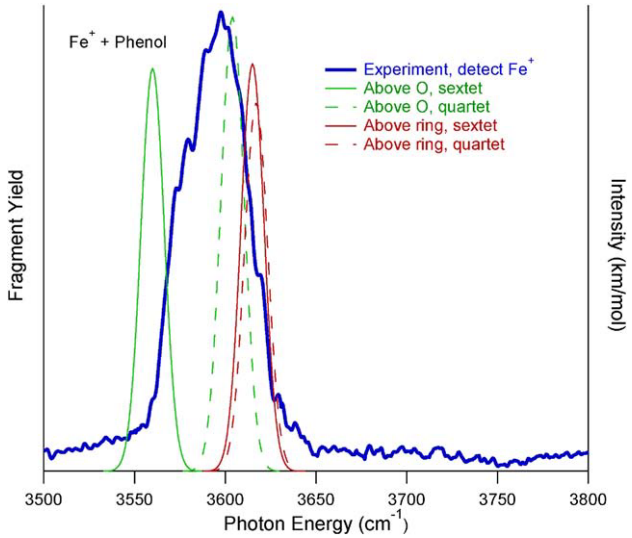

Figure 4. Experimental and calculated vibrational spectra of $Fe^+(C_6H_5OH)$ in the O–H stretching region. The experimental spectrum is obtained by IRMPD of ions produced by reacting Fe^+ with C_6H_5OH and monitoring Fe^+ fragments (blue). Calculated spectra (right axis) are at the B3LYP/6-311+G(d,p) level, with frequencies scaled by 0.954. Spectra of $Fe^+(C_6H_5OH)$ with Fe^+ bound to the oxygen (σ-complex) and above the ring (π-complex) are shown. For the simulations, solid lines represent sextet states and dashed lines quartet states.

been measured in the O–H stretching region. Spectra of the quartet and sextet states of $[HO\text{-}Fe\text{-}C_6H_5]^+$, the key insertion intermediate, are obtained from IRMPD, monitoring the $FeOH^+$ fragment. With the aid of B3LYP/6-311+G(d,p) calculations the main peak observed at 3700 cm^{-1} is assigned to the sextet state and the shoulder at ~3670 cm^{-1} to the quartet state. IRMPD of the $Fe^+(C_6H_5OH)$ exit channel complex primarily produces $Fe^+ + C_6H_5OH$; $Fe^+(C_6H_4) + H_2O$ is a minor product. The spectrum consists of a peak at 3598 cm^{-1}. Calculations suggest that it is due to the quartet $Fe^+(C_6H_5OH)$ π-complex, although the sextet π-complex and the quartet σ-complex could also contribute. The spectrum of ions produced by reacting Fe^+ with N_2O and benzene is narrower than that obtained using Fe^+ + phenol. This could be due to different populations of the isomers or to different vibrational temperatures in the two cases. In addition, a potential energy surface for the reaction has been calculated at the CBS-QB3 level.

Acknowledgments

The authors gratefully acknowledge financial support from the National Science Foundation under awards CHE-0608446 and CHE-0911225.

References

1. Svobodová, A.; Psotová, J.; Walterová, D. Natural Phenolics in the Prevention of UV-Induced Skin Damage. A Review. *Biomed. Papers* **2003,** *147,* 137–145.
2. Panov, G. I. Advances in Oxidation Catalysis: Oxidation of Benzene to Phenol by Nitrous Oxide. *Cat Tech* **2000,** *4,* 18–31.
3. Taboada, J. B. Direct Oxidation of Benzene to Phenol: Investigation of the Active Iron Species in [Fe,Al]MFI Catalysts by ^{57}Fe Mössbauer Spectroscopy; Delft University Press: Amsterdam, 2006; p. 172.
4. Niwa, S.; Eswaramoorthy, M.; Nair, J.; Raj, A.; Itoh, N.; Shoji, H.; Namba, T.; Mizukami, F. A One-Step Conversion of Benzene to Phenol with a Palladium Membrane. *Science* **2002,** *295,* 105–107.
5. Tao, Y.; Fishman, A.; Bentley, W. E.; Wood, T. K. Oxidation of Benzene to Phenol, Catechol, and 1,2,3-Trihydroxybenzene by Toluene 4-Monooxygenase of *Pseudomonas mendocina* KR1 and Toluene 3-Monooxygenase of *Ralstonia pickettii* PKO1. *Appl. Environ. Microbiol.* **2004,** *70,* 3814–3820.
6. Schlosser, P. M.; Bond, J. A.; Medinsky, M. A. Benzene and Phenol Metabolism by Mouse and Rat-Liver Microsomes. *Carcinogenesis* **1993,** *14,* 2477–2486.
7. Ortiz de Montellano, P. R. *Cytochrome P450: Structure, Mechanism, and Biochemistry*, 3rd ed.; Kluwer Academic/Plenum Publishers: New York, 2004, pp 45–114.
8. Ryan, M. F.; Stockigt, D.; Schwarz, H. Oxidation of Benzene Mediated by First-Row Transition-Metal Oxide Cations—the Reactivity of ScO^+ through NiO^+ in Comparison. *J. Am. Chem. Soc.* **1994,** *116,* 9565–9570.
9. Schröder, D.; Schwarz, H. Benzene Oxidation by 'Bare' FeO^+ in the Gas Phase. *Helv. Chim. Acta* **1992,** *75,* 1281–1287.
10. Becker, H.; Schröder, D.; Zummack, W.; Schwarz, H. Generation, Fragmentation, and Interconversion Processes of $[Fe,C_6,H_6,O]^+$ Isomers Relevant for the Oxygenation of Aromatic Hydrocarbons. *J. Am. Chem. Soc.* **1994,** *116,* 1096–1100.
11. Yoshizawa, K.; Shiota, Y.; Yamabe, T. Reaction Pathway for the Direct Benzene Hydroxylation by Iron-Ore Species. *J. Am. Chem. Soc.* **1999,** *121,* 147–153.
12. Yoshizawa, K.; Shiota, Y.; Kagawa, Y.; Yamabe, T. Femtosecond Dynamics of the Methane-Methanol and Benzene-Phenol Conversions by an Iron-Oxo Species. *J. Phys. Chem. A* **2000,** *104,* 2552–2561.
13. Shiota, Y.; Suzuki, K.; Yoshizawa, K. Mechanism for the Direct Oxidation of Benzene to Phenol by FeO+. *Organometallics* **2005,** *24,* 3532–3538.
14. Kwapien, K.; Broclawik, E. Interaction of FeO^+ Cation with Benzene, Aniline, and 3-Methylaniline: DFT Study of Oxygen Insertion Mechanism. *Int. J. Quantum Chem.* **2008,** *108,* 2016–2022.
15. Altinay, G., Citir, M., Metz, R. B. Vibrational Spectroscopy of Intermediates in Methane-to-Methanol Conversion by FeO^+. Unpublished, (submitted 2010).
16. Aguirre, F.; Husband, J.; Thompson, C. J.; Stringer, K. L.; Metz, R. B. Electronic Spectroscopy of Intermediates Involved in the Conversion of Methane to Methanol by FeO^+. *J. Chem. Phys.* **2002,** *116,* 4071–4078.
17. Metz, R. B. Photofragment Spectroscopy of Covalently Bound Transition Metal Complexes: A Window into C–H and C–C Bond Activation by Transition Metal Ions. *Int. Rev. Phys. Chem.* **2004,** *23,* 79–108.
18. Husband, J.; Aguirre, F.; Ferguson, P.; Metz, R. B. Vibrationally Resolved. Photofragment Spectroscopy of FeO^+. *J. Chem. Phys.* **1999,** *111,* 1433–1437.
19. Aguirre, F.; Husband, J.; Thompson, C. J.; Stringer, K. L.; Metz, R. B. The Low-Lying Electronic. States of FeO^+: Rotational Analysis of the Resonance Enhanced Photodissociation Spectra of the $^6\Pi_{7/2} - {}^6\Sigma^+$ System. *J. Chem. Phys.* **2003,** *119,* 10194–10201.
20. Kaur, D.; Desouza, A. M.; Wanna, J.; Hammad, S. A.; Mercorelli, L.; Perry, D. S. Multipass Cell for Molecular-Beam Absorption-Spectroscopy. *Appl. Optics* **1990,** *29,* 119–124.
21. Frisch, M. J.; Trucks, G. W.; Schlegel, H. B.; Scuseria, G. E.; Robb, M. A.; Cheeseman, J. R.; Montgomery, J. A. Jr.; Vreven, T.; Kudin, K. N.; Burant, J. C.; Millam, J. M.; Iyengar, S. S.; Tomasi, J.; Barone, V.; Mennucci, B.; Cossi, M.; Scalmani, G.; Rega, N.; Petersson, G. A.; Nakatsuji, H.; Hada, M.; Ehara, M.; Toyota, K.; Fukuda, R.; Hasegawa, J.; Ishida, M.; Nakajima, T.; Honda, Y.; Kitao, O.; Nakai, H.; Klene, M.; Li, X.; Knox, J. E.; Hratchian, H. P.; Cross, J. B.; Adamo, C.; Jaramillo, J.; Gomperts, R.; Stratmann, R. E.; Yazyev, O.; Austin, A. J.; Cammi, R.; Pomelli, C.; Ochterski, J. W.; Ayala, P. Y.; Morokuma, K.; Voth, G. A.; Salvador, P.; Dannenberg, J. J.; Zakrzewski, V. G.; Dapprich, S.; Daniels, A. D.; Strain, M. C.; Farkas, O.; Malick, D. K.; Rabuck, A. D.; Raghavachari, K.; Foresman, J. B.; Ortiz, J. V.; Cui, Q.; Baboul, A. G.; Clifford, S.; Cioslowski, J.; Stefanov, B. B.; Liu, G.; Liashenko, A.; Piskorz, P.; Komaromi, I.; Martin, R. L.; Fox, D. J.; Keith, T.; Al-Laham, M. A.; Peng, C. Y.; Nanayakkara, A.; Challacombe, M.; Gill, P. M. W.; Johnson, B.; Chen, W.; Wong, M. W.; Gonzalez, C.; Pople, J. A. *Gaussian* 03; Gaussian, Inc.: Pittsburgh PA, Wallingford, CT, 2004.
22. Montgomery, J. A. Jr.; Frisch, M. J.; Ochterski, J. W.; Petersson, G. A. A Complete Basis Set Model Chemistry. VI. Use of Density Functional Geometries and Frequencies. *J. Chem. Phys.* **1999,** *110,* 2822–2827.
23. Montgomery, J. A. Jr.; Frisch, M. J.; Ochterski, J. W.; Petersson, G. A. A Complete Basis Set Model Chemistry. Use of the Minimum Population Localization Method. *J. Chem. Phys.* **2000,** *112,* 6532–6542.
24. Kellogg, C. B.; Irikura, K. K. Gas-Phase Thermochemistry of Iron Oxides and Hydroxides: Portrait of a Super-efficient Flame Suppressant. *J. Phys. Chem. A* **1999,** *103,* 1150–1159.
25. Glukhovtsev, M. N.; Bach, R. D.; Nagel, C. J. Performance of the B3LYP/ECP DFT Calculations of Iron-Containing Compounds. *J. Phys. Chem. A* **1997,** *101,* 316–323.
26. Feller, D. Ab Initio Study of M^+:18-Crown-6 Microsolvation. *J. Phys. Chem. A* **1997,** *101,* 2723–2731.
27. Metz, R. B.; Nicolas, C.; Ahmed, M.; Leone, S. R. Direct Determination of the Ionization Energies of FeO and CuO with VUV Radiation. *J. Chem. Phys.* **2005,** *123,* 114313.

28. Armentrout, P. B.; Kickel, B. L. Gas-Phase Thermochemistry of Transition Metal Ligand Systems: Reassessment of Values and Periodic Trends. In *Organometallic Ion Chemistry*; Freiser, B. S., Ed.; Kluwer Academic Publishers: Dordrecht, The Netherlands, 1994; p. 1–45.
29. Lias, S. G.; Bartmess, J. E.; Liebman, J. F.; Holmes, J. L.; Levin, R. D.; Mallard, W. G. Gas-Phase Ion and Neutral Thermochemistry. *J. Phys. Chem. Ref. Data.* **1988,** *17,* 1–861.
30. Schröder, D.; Schwarz, H. FeO^+ Activates Methane. *Angew. Chem. Int. Ed. Engl.* **1990,** *29,* 1433–1434.
31. Schröder, D.; Schwarz, H.; Clemmer, D. E.; Chen, Y.; Armentrout, P. B.; Baranov, V.; Bohme, D. K. Activation of Hydrogen and Methane by Thermalized FeO^+ in the Gas Phase as Studied by Multiple Mass Spectrometric Techniques. *Int. J. Mass Spectrom. Ion Processes* **1997,** *161,* 175–191.
32. Yamada, Y.; Ebata, T.; Kayano, M.; Mikami, N. Picosecond I R-UV Pump-Probe Spectroscopic Study of the Dynamics of the Vibrational Relaxation of Jet-Cooled Phenol. I. Intramolecular Vibrational Energy Redistribution of the OH and CH Stretching Vibrations of Bare Phenol. *J. Chem. Phys.* **2004,** *120,* 7400–7409.
33. Park, M.; Hauge, R. H.; Kafafi, Z. H.; Margrave, J. L. Activation of O–H and C–O Bonds of Methanol by Photoexcited Iron Atoms. *J. Chem. Soc. Chem. Commun.* **1985,** 1570–1571.
34. Wang, G. J.; Chen, M. H.; Zhou, M. F. Matrix Isolation Infrared Spectroscopic and Theoretical Studies on the Reactions of Manganese and Iron Monoxides with Methane. *J. Phys. Chem. A* **2004,** *108,* 11273–11278.
35. Baranov, V.; Javahery, G.; Hopkinson, A. C.; Bohme, D. K. Intrinsic Coordination. Properties of Iron in FeO^+: Kinetics at 294 ± 3 K for Gas-Phase Reactions of the Ground States of Fe^+ and FeO^+ with Inorganic Ligands Containing Hydrogen, Nitrogen, and Oxygen. *J. Am. Chem. Soc.* **1995,** *117,* 12801–12809.
36. Stockigt, D.; Schwarz, H. Reactivity Tuning by Ligand Effects—Gas-Phase Reactions of $Fe(C_6H_6)O^+$ Versus Bare FeO^+. *Chemische Berichte* **1994,** *127,* 2499–2503.
37. Baranov, V.; Bohme, D. K. Reactions of Fe^+ Coordinated to the Pi-Donating Ligands C_2H_4, c-C_5H_5, C_6H_6, and C_{60} with N_2O and CO-Probing the Bonding in $(C_{60})Fe^+$. *Int. J. Mass Spectrom. Ion Process* **1995,** *149,* 543–553.
38. Meyer, F.; Khan, F. A.; Armentrout, P. B. Thermochemistry of Transition-Metal Benzene Complexes-Binding-Energies of $M(C_6H_6)(X)^+$ (X = 1, 2) for M=Ti to Cu. *J. Am. Chem. Soc.* **1995,** *117,* 9740–9748.
39. Vaden, T. D.; Lisy, J. M. Characterization of Hydrated Na^+(Phenol) and K^+(Phenol) Complexes Using Infrared Spectroscopy. *J. Chem. Phys.* **2004,** *120,* 721–730.
40. Amunugama, R.; Rodgers, M. T. The Influence of Substituents on Cation-π Interactions. 4. Absolute Binding Energies of Alkali Metal Cation–Phenol Complexes Determined by Threshold Collision-Induced Dissociation and Theoretical Studies. *J. Phys. Chem. A* **2002,** *106,* 9718–9728.
41. Lagutschenkov, A.; Sinha, R.K.; Maitre, P.; Dopfer, O. Structure and Infrared Spectrum of the Ag^+-Phenol Ionic Complex. Unpublished, (submitted 2010).